THE JOURNAL OF PHYSICAL CHEMISTRY B
A JOURNAL OF THE AMERICAN CHEMICAL SOCIETY

pubs.acs.org/JPCB

Article

Incoherent Nonreciprocal Absorbance Circular Dichroism of Uniaxial Assemblies

Gwendylan A. Turner, Yechan Hwang, Jiayue Rong, Camila Strachan, and Garth J. Simpson*

Cite This: J. Phys. Chem. B 2023, 127, 8216–8225

Read Online

ACCESS | Metrics & More | Article Recommendations | Supporting Information

ABSTRACT: Analytical theory is proposed predicting remarkably large and fully electric-dipole-allowed circular dichroism (CD) in electronic ultraviolet−visible (UV−vis) absorbance spectroscopy of uniaxial surface assemblies. Partial depolarization of the transmitted beam provides a pathway for surface-specific and chiral-specific dissymmetry parameters that are orders of magnitude greater than those from analogous measurements of isotropic systems. Predictions of the model generated using ab initio quantum chemical calculations with no adjustable parameters agreed with UV−vis absorbance CD measurements of naproxen microcrystals prepared on hydrophilic substrates. Notably, these calculations correctly predicted (i) the key spectroscopic features, (ii) the relative magnitudes of chiral-specific peaks in the CD spectrum, (iii) the absolute CD sign, and (iv) the reciprocal CD sign inversion arising from sample reorientation in the instrument. These results connect the molecular structure and orientation to large CD observable in oriented thin-film assemblies, with the potential for further extension to broad classes of chiral-specific spectral analyses.

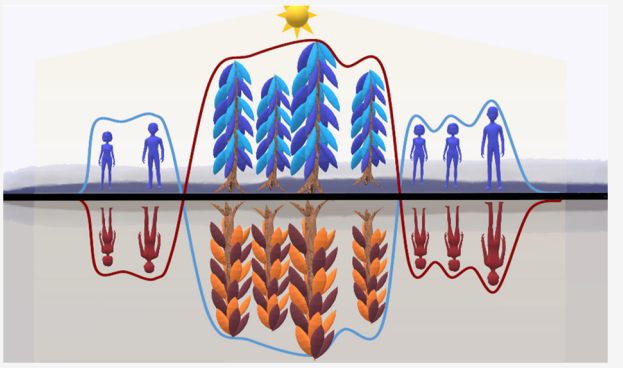

INTRODUCTION

Molecular and supramolecular chirality play critical roles in the formation and interactions of biological systems, accessed experimentally through chiroptical spectroscopies. Chiral-specific perturbations in spectral analysis are typically orders of magnitude weaker in isotropic media than their achiral counterparts, complicating their analytical utility. While the relationships between molecular chirality and circular dichroism (CD) absorbance spectroscopy have been studied for over a century for isotropic systems, predictive models for ordered assemblies of lower symmetry are less well-established. However, additional electric-dipole-allowed mechanisms for chiral-specific effects can arise in ordered assemblies. Most theoretical and experimental approaches on this subject focus on methods to remove these presumed "artifacts" from local ordering to isolate the isotropic response. Notably, the combined effect of linear dichroism and linear birefringence (LD−LB) in anisotropic media has been known for more than 30 years to produce electric-dipole-allowed CD responses in ordered systems that are unique from the isotropic responses.[1−4] Notably, the sign of the CD response arising from LD−LB effects inverts in sign upon sample flipping, dubbed a reciprocal CD response. In anisotropic samples, Shindo proposed a Mueller/Stokes formalism for decomposing the observed CD response to contributions from isotropic CD (nonreciprocal), LD−LB interactions (reciprocal), LD, and polarization-dependent detection artifacts.[5]

However, these "interferences" from LD−LB interactions can often exhibit sensitivity to chirality orders of magnitude greater than the isotropic counterparts.[4] While this higher sensitivity often frustrates isolation of the isotropic response, it simultaneously suggests intriguing possibilities for improvement in chiral-specific selectivity and sensitivity. The analytical utility of this orders-of-magnitude improvement in chiral sensitivity arguably hinges on the reliability of predictive frameworks to connect the observables back to the molecular structure and orientation. Major strides toward this end have appeared recently from work by Salij, Goldsmith, and Tempelaar,[6] in which a molecular basis was proposed for describing LD−LB contributions to CD in terms of interactions through consideration of a pair of local Lorentz oscillators within the molecular frame. In particular, Salij et al. identified the importance at the molecular level of non-coparallel transition moments,[6] consistent with analogous prior conclusions at the macroscopic material level requiring orientational disparities between the principal axes describing

Received: May 10, 2023
Revised: June 23, 2023
Published: September 18, 2023

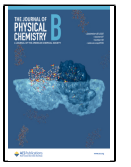

LD and LB in order for the pairing to produce interferences in CD measurements.[3]

Intriguingly, several recent studies have reported experimental observation of nonreciprocal CD attributed to LD−LB effects in samples exhibiting neither LD nor LB. In studies by Albano, di Bari, and co-workers,[7] thin films of an oligothiophene were shown to exhibit large dissymmetry parameters ($g \cong \pm 0.2$) with nearly total sign inversion upon sample flipping but negligible net linear dichroism. Nevertheless, the sign inversion upon sample reorientation together with the large dissymmetry parameter suggested a dominance from LD−LB effects. Microscopy of the resulting thin films identified local domains extending over distances large relative to the wavelength of light but small relative to the probed area of the spectrometer. In this case, LD−LB contributions were attributed to optical interactions within localized organized domains. In measurements of binaphthol thin films by Kartouzian and co-workers,[8] nonreciprocal CD emerged upon storage of evaporated thin films upon crystal formation. Optical micrographs suggested the formation of locally ordered crystalline domains with persistence lengths of order spanning up to several millimeters. However, in the absence of net LD or LB upon sample rotation, the authors attributed the signal to isotropic CD but provided little explanation for the CD sign inversion upon sample flipping without chiral inversion within the molecular frame. In follow-up measurements by second-harmonic generation circular dichroism (SHG-CD),[9] Kartouzian and co-workers cited the advantage of using large-beam measurements to integrate over local anisotropic domains in SHG-CD measurements acquired at normal incidence. In closely related work, circularly polarized emission with anisotropy parameters around ±10% was reported by di Bari and co-workers, also attributed to the formation of domains exhibiting local anisotropy.

Despite the success of the model by Salij et al., ambiguities in the molecular packing within the oligothiophene molecules at the interface arguably complicate definitive validation of the proposed orientational mechanism. While simulations support the possibility of observing CD spectral measurements for assemblies with particular assumed molecular orientations, nonlinear fitting of the spectral and molecular properties was performed to align the predicted and measured spectral responses; it is not clear whether these presumed orientation distributions are consistent with the molecular ordering produced upon drop-casting thin oligothiophene films. Furthermore, Salij et al. correctly conclude that circular polarization is in principle agnostic to the principal direction of a locally ordered domain, but did not explicitly consider the collective effects of many such domains on the polarization dependence of the net transmitted beam. While providing a solid foundation for interpreting these spectral features, the framework of Salij et al. would be further strengthened through derivation of formal symmetry-derived molecular and supramolecular requirements bridging molecular chirality, supramolecular chirality, and the macroscopic CD observables. Ideally, one would seek to identify a molecular assembly, in which both the molecular structure and the supramolecular packing within the local material can be known a priori for direct comparison between theory and experiment without adjustable fitting parameters.

The observation of apparent LD−LB contributions to CD by Albano and co-workers in assemblies exhibiting no net LB or LD[7] suggests potential merit in considering spectroscopic analyses in systems of higher symmetry than typically attributed to LD−LB coupling. When considering predictive frameworks for system symmetries approaching isotropic, the most obvious starting point is arguably uniaxial, in which one axis is unique relative to the other two orthogonal axes. Uniaxial symmetry is by far the most prevalent below isotropic, routinely arising at interfaces, in fibrillar macromolecular assemblies, in lamellar structures, in systems under flow, and in the presence of applied external fields. Furthermore, uniaxial symmetry with a unique axis normal to the surface is consistent with the absence of both linear dichroism and linear birefringence measured along the surface normal, consistent with the LD−LB attributed measurements reported by Albano and co-workers.[7]

While a fair body of work has been considered LD−LB contributions to local chirality in coherent transmission measurements for anisotropic samples, comparatively little has been devoted analysis in the incoherent limit in azimuthally isotropic samples. Decoherence is generally driven by fluctuations in optical phase and/or polarization as a function of time, position, or both. In isotropic systems, decoherence routinely arises in the presence of light scattering, in which measurements typically integrate over dynamic fluctuations within the probe volume. In spatially structured samples, optical scattering and/or microscopy provides access to contrast related to spatial fluctuations, in which integration in space results in coherence loss in optical transmission. In both instances, loss in coherence is more pronounced when the persistence length of local or transient order approaches or exceeds the optical wavelength.

The presence of partial decoherence can also impact both the scaling and orientation dependence of the detected intensity. Optical signals produced from coherent interactions in condensed-phase molecular materials generally scale quadratically with molecular number density. Such operations can be described using Jones vectors and matrices, with optical interactions fully defined by field-based descriptions of polarization.[10,11] In contrast, incoherent interactions such as those from molecular scattering result in a linear scaling with number density. These scaling trends are also mirrored in the orientational averages connecting the detected intensities back to molecular orientation. A classic example from nonlinear optics is the difference in symmetry and orientational averaging for coherent second-harmonic generation, which is symmetry forbidden from orientational averaging in isotropic media as an even-ordered three-wave mixing process, contrasted with hyper-Rayleigh scattering, which is the incoherent analog and bulk-allowed when cast as a six-wave mixing process.[12−14] Rather than field-based Jones transformation matrices, Stokes vectors and Mueller matrices are more useful for describing polarization transfer in partially decohering light/matter interactions. In the orientation dependence, a quadratic scaling with number density for coherent interactions results in expressions for the orientational average scaling linearly with the molecular polarizability. In contrast, the linear scaling with number density for incoherent interactions correspondingly yields a quadratic scaling in the orientational averaging over the molecular polarizability. Importantly, this difference in the molecular orientation dependence for coherent versus incoherent interactions can influence the connections bridging far-field observables to local and molecular-scale properties.

In this context, mathematical approaches for describing the orientational averages for coherent four-wave mixing spectro-

https://doi.org/10.1021/acs.jpcb.3c03104
J. Phys. Chem. B 2023, 127, 8216−8225

scopic observables in uniaxial assemblies have the potential to map directly onto incoherent two-wave mixing spectroscopy. In this case, our prior work describing selection rules and symmetry relations for four-wave mixing spectroscopy in uniaxial assemblies[15] may potentially be brought to bear for describing incoherent contributions to absorption spectroscopy. Notably, prior work predicted the possibility of observing fully electric-dipole chiral-specific and interface-specific four-wave mixing (4WM).[15] The primary purpose of this study is to explore the predictive capability of this prior electric-dipole-allowed four-wave mixing framework in quantitatively recovering chiral-specific observables in absorption spectroscopy of oriented assemblies with a known molecular and macromolecular structure.

METHODS

Experimental Methods. Thin films of (*R*)- and (*S*)-naproxen were prepared by drop-coating microcrystalline suspensions onto hydrophilic fused silica microscope slides. Fused silica microscope slides (Esco Optics) were cut for compatibility with the spectrometer sample chamber width (12.5 mm). Slide surfaces were prepared by immersion in "piranha" solution consisting of three parts concentrated sulfuric acid to one part 35% peroxide solution at 60 °C for 30 min to provide a uniform hydrophilic surface. Enantiomerically pure microcrystalline suspensions of naproxen (98% purity; MilliporeSigma) in saturated toluene were then prepared at 7.00 mg/mL at 40 °C for crystal deposition, cooled to room temperature, deposited dropwise onto slide surfaces, and left for slow evaporation in a desiccator. Brightfield images of the resulting films were taken at 10× magnification to extract domain sizes. Second-harmonic generation imaging (Formulatrix SONICC) confirmed the presence of homochiral crystals by this preparation. Domain sizes were estimated by obtaining the power spectrum of the corresponding brightfield images, fitting the resulting autocorrelogram with exponential decay, and extracting the characteristic spatial frequency.

The crystalline thin films were oriented with the slide perpendicular to the optical axis during absorbance and CD measurements. Samples in the "normal" orientation were taken with the thin film facing toward the light source. The slides were then rotated 180° about the axis perpendicular to the principal axis to the "flipped" orientation and again measured. All CD and absorbance measurements were obtained using a J-1500 circular dichroism spectrometer with a scanning speed of 50 nm/min and a digital integration time of 4 s. Microcrystalline suspensions of (*R*)- and (*S*)-naproxen were prepared at 4.00 mM in hexanes, and absorbance and CD measurements were performed using a standard 1 mm path length fused-silica cuvette (Starna Cells).

Quantum calculations of (*S*)-naproxen were performed using the GAMESS electronic structure package, version 2016 R1.[19] The initial molecule structure was imported from the Cambridge Structural Database (CSD)[20] using the structure reported previously[21] and referenced by CSD identifier COYRUD. The transition dipole moment of excited states 1−10 and the adiabatic polarizability were calculated using DFT(B3LYP) with a 6-31G* basis set. Visualization of the molecular orbitals was conducted using MacMolPlt.[22] Calculations were performed in a dielectric continuum to partially account for the local environment within crystalline lattice.

Theoretical Foundation. *Jones Framework.* The electric polarization **P** induced from a material is given by the product of the local electric field and the electric susceptibility matrix χ. In this local frame, the electric field is described by a 3 × 1 column vector in Cartesian coordinates. In the limit of a thin film, the subscript eff indicates the effective field experienced locally within the dielectric environment within the film.

$$\mathbf{P}^{\omega} = \chi_{\text{eff}} \mathbf{e}_{\text{in}}^{\omega} \tag{1}$$

Provided the path length is sufficiently short such that the change in polarization by the sample is negligible, the eff moniker can be removed by incorporating local Fresnel factor corrections through multiplication by a diagonal matrix **L**, which bridges the far-field polarization to the local driving fields. For measurements at normal incidence in a macroscopically uniaxial system about the surface normal *Z*-axis, the Fresnel factor corrections for the *X*- and *Y*-polarized fields are identical with $L^{xx} = L^{yy}$.

$$\mathbf{P} = \chi \mathbf{L}^{\text{in}} \mathbf{e}^{\text{in}} \tag{2}$$

The polarization dependence of the detected field is connected to the induced polarization by projection onto the detected polarization state for a given geometry of detection. For coherent plane-wave light at normal incidence, only the *X* and *Y* field components at the interface are nonzero.

$$\mathbf{e}^{\text{out}} = \mathbf{L}^{\text{out}} \mathbf{P} \tag{3}$$

For measurements of uniaxial systems at normal incidence, the equality between L^{xx} and L^{yy} allows the matrices $\mathbf{L}^{\text{in}}$ and $\mathbf{L}^{\text{out}}$ to be replaced by the scalar multipliers L^{in} and L^{out}, respectively.

It is worth noting that this framework does not account for perturbations from local birefringence within the Fresnel local field factors themselves. However, the role of linear birefringence is explicitly considered in the formulation of the local polarizability matrix χ. This approach more conveniently connects the observables from the thin-film assembly back to molecular properties.

Mueller/Stokes Framework. In structurally heterogeneous films with persistence lengths significantly greater than the wavelength of light, the combined transmitted intensity consists of the incoherent addition of the intensities produced by many individual locations when detected on an integrating detector. Formally, the separate sources will produce a speckle pattern, as the local fields add to produce interference. However, integration over the speckle pattern leads to an incoherent summation of the combined intensities. In this case, it is more practically useful to describe the detected polarization state integrated over the probe area of the beam in terms of Stokes vectors and Mueller matrices rather than Jones vectors and matrices.

$$\mathbf{s}_{\text{out}}^{\omega} = \mathbf{A}(\mathbf{e}_{\text{out}}^{\omega^*} \otimes \mathbf{e}_{\text{out}}^{\omega}) \tag{4}$$

The matrix **A** connects the Kronecker product (indicated by the ⊗ operation) of Jones vectors for the fields with the Stokes vector.[10]

Substituting for the (un-normalized) Stokes vector using eq 4 and replacing the matrices **L** with constants (consistent with measurements made along the macroscopic uniaxial axis) yield the following expression for the Stokes vector describing the polarization state of the transmitted beam in a framework amenable to incorporation of partial depolarization.

https://doi.org/10.1021/acs.jpcb.3c03104
J. Phys. Chem. B 2023, 127, 8216−8225

$$\mathbf{s}^{\text{out}} = |L^{\text{out}}|^2|L^{\text{in}}|^2\mathbf{A}[(\chi^{(1)}\mathbf{e}^{\text{in}})^* \otimes (\chi^{(1)}\mathbf{e}^{\text{in}})] \quad (5)$$

Using the relation $(a\cdot b) \otimes (c\cdot d) = (a \otimes c)\cdot(b \otimes d)$, the expression in eq 5 can be rewritten as follows

$$\mathbf{s}^{\text{out}} = |L^{\text{out}}|^2|L^{\text{in}}|^2\mathbf{A}(\chi^* \otimes \chi)(\mathbf{e}^{\text{in}^*} \otimes \mathbf{e}^{\text{in}}) \quad (6)$$

Macroscopic Uniaxial Assemblies. In the limit of relatively weak intermolecular electronic interactions and assuming intermolecular distances much smaller than the wavelength of light, the total electric susceptibility for a bulk material is given by coherent summation of the collective polarizability contributions of each molecule, in turn described by the matrix $\boldsymbol{\alpha}$. For identical molecules differing only in their orientation, this coherent summation corresponds to the following orientational average.

$$\chi^{IJ} \cong \frac{N_b}{\varepsilon_0}\sum_{i,j}\langle R_{Ii}R_{Jj}\rangle\alpha_{00}^{ij} \quad (7)$$

In eq 7, R refers to a coordinate transformation matrix connecting the molecular frame (indicated by lowercase prime indices) to the interfacial frame of the thin-film assembly (indicated by uppercase Cartesian coordinates) and α^{ij} refers to the ij element of the molecular polarizability matrix $\boldsymbol{\alpha}$. For coherent optical interactions based on direct detection of the optical field (including purely polarized polarization states measured using Jones vectors), the orientational averages are performed over just the two indices given in eq 7. Coherent interactions throughout the medium also result in a quadratic scaling with number density N_b from the squared modulus of eq 7.

The orientational averaging results in notable differences for summation over the intensities for incoherent interactions rather than coherent interactions from a single isolated domain. By analogy with second-harmonic generation, coherent SHG results from averaging over a set of three rotation matrices for describing the observables, while the incoherent analog of hyper-Rayleigh scattering is described by orientational averages evaluated over combinations of six rotation matrices.[12−14] In the case of observables derived from incoherent addition of the intensities as can arise from measurements of a locally heterogeneous surface assembly, the orientational averages are analogously evaluated over the products of $\chi^* \otimes \chi$ in eq 6, the individual elements of which are given below.

$$\chi^{IJ^*}\chi^{KL} = \sum_{i,j,k,l=x,y,z}\left(\frac{N_b}{\varepsilon_0}\right)\langle R_{Ii}R_{Jj}R_{Kk}R_{Ll}\rangle(\alpha^{ij^*}\alpha^{kl}) \quad (8)$$

In eq 8, N_b is the bulk number density and ε_0 is the vacuum permittivity. Incoherent summations can arise from integrating over signals produced by assemblies of structures spaced distances significantly greater than the wavelength of light (e.g., in microscopy measurements) or from dynamic fluctuations in position. Incoherent summation results in a linear scaling with number density instead of a quadratic and an orientational average evaluated over products of four rotation matrices for optical transmission rather than just two.

For molecular solids and liquids, the susceptibility of the material can be initially approximated by summation over the molecular polarizability. The polarizability matrix describing the linear optical properties of a single molecule is given from perturbation theory as sum-over-states.[16]

$$\alpha_{00}^{ij}(-\omega, \omega) = \frac{1}{\hbar}\sum_{n=0}^{\infty}\frac{\mu_{0n}^{i}\mu_{n0}^{j}}{\omega_n - \omega - i\Gamma_n} + \frac{\mu_{0n}^{j}\mu_{n0}^{i}}{\omega_n + \omega + i\Gamma_n} \quad (9)$$

The expression above for a single molecule can also be used to describe molecular assemblies, including crystals and thin films.

The orientational averages described in eq 8 above naturally account for the symmetry properties expected within isotropic and uniaxial assemblies. In macroscopically isotropic systems, the following set of unique, nonzero tensor products are allowed by symmetry: $\chi^{II*}\chi^{II}$, $\chi^{II*}\chi^{JJ}$, $\chi^{IJ*}\chi^{IJ}$, and $\chi^{IJ*}\chi^{JI}$. For a symmetric molecular polarizability matrix consistent with absorption and transmission, the last two products become equivalent, leading to a maximum of three unique polarization-dependent observables accessible in isotropic assemblies. The introduction of chirality within the molecular frame does not change the set of allowed combinations described above within the electric dipole approximation for light.

For uniaxial achiral assemblies (D_∞, $D_{\infty h}$, and $C_{\infty v}$ symmetries), the number of unique polarizability combinations increases to 11, 10 of which are independent; $f_{12} = \chi^{XX*}\chi^{YY} = \chi^{YY*}\chi^{XX}$, $f_{13} = \chi^{XX*}\chi^{ZZ} = \chi^{YY*}\chi^{ZZ}$, $f_{31} = \chi^{ZZ*}\chi^{XX} = \chi^{ZZ*}\chi^{YY}$, $f_{33} = \chi^{ZZ*}\chi^{ZZ}$, $f_{44} = \chi^{YX*}\chi^{XY} = \chi^{YX*}\chi^{YX}$, $f_{45} = \chi^{XY*}\chi^{YX} = \chi^{YX*}\chi^{XY}$, $f_{66} = \chi^{XZ*}\chi^{XZ} = \chi^{YZ*}\chi^{YZ}$, $f_{67} = \chi^{XZ*}\chi^{ZX} = \chi^{YZ*}\chi^{ZY}$, $f_{76} = \chi^{ZX*}\chi^{XZ} = \chi^{ZY*}\chi^{YZ}$, and $f_{77} = \chi^{ZX*}\chi^{ZX} = \chi^{ZY*}\chi^{ZY}$, with $f_{11} = \chi^{XX*}\chi^{XX} = \chi^{YY*}\chi^{YY} = \chi^{XX*}\chi^{YY} + \chi^{XY*}\chi^{XY} + \chi^{XY*}\chi^{YX}$.[15,17] Relaxing the symmetry to C_∞ yields an additional 10 new unique chiral-specific polarizability combinations allowed within the electric dipole approximation, 9 of which are independent; $f_{14} = \chi^{XX}\chi^{XY} = -\chi^{YY*}\chi^{YX}$, $f_{41} = \chi^{XY*}\chi^{XX} = -\chi^{YX*}\chi^{YY}$, $f_{15} = \chi^{XX*}\chi^{YX} = -\chi^{YY*}\chi^{XY}$, $f_{34} = \chi^{ZZ*}\chi^{XY} = -\chi^{ZZ*}\chi^{YX}$, $f_{43} = \chi^{XY*}\chi^{ZZ} = -\chi^{YX*}\chi^{ZZ}$, $f_{68} = \chi^{XZ*}\chi^{YZ} = -\chi^{YZ*}\chi^{XZ}$, $f_{79} = \chi^{ZX*}\chi^{ZY} = -\chi^{ZY*}\chi^{ZX}$, $f_{69} = \chi^{XZ*}\chi^{ZY} = -\chi^{YZ*}\chi^{ZX}$, $f_{96} = \chi^{ZY*}\chi^{XZ} = -\chi^{ZX*}\chi^{YZ}$, with $f_{51} = \chi^{YX*}\chi^{XX} = -\chi^{XY*}\chi^{YY} = -(\chi^{XY*}\chi^{XX} + \chi^{XX*}\chi^{YX} + \chi^{XX*}\chi^{XY})$. These chiral-specific elements were first reported for four-wave mixing by Davis et al.[15] and were subsequently used to describe the origins of high-sensitivity chiral-specific fluorescence arising in uniaxial interfacial assemblies.[17]

The CD response can be connected back to these symmetry-allowed chiral-specific susceptibility products summarized in the Supporting Information by considering the Stokes vectors produced for right versus left circularly polarized incident light. For normal incidence, only the (X,Y) fields and corresponding elements of χ need to be considered explicitly. The Kronecker product $(\mathbf{e}^{\text{in}*} \otimes \mathbf{e}^{\text{in}})$ is given by the following expression, for $\mathbf{e}_{R/L} = \frac{1}{\sqrt{2}}[1, \pm i]$.

$$(\mathbf{e}_{R/L}^{\text{in}^*} \otimes \mathbf{e}_{R/L}^{\text{in}}) = \frac{1}{2}\begin{bmatrix}1\\ \pm i\\ \mp i\\ 1\end{bmatrix} \quad (10)$$

Substitution into eq 6 in combination with the symmetry relations for uniaxial systems yields the following expression for the Stokes vector.

$$\mathbf{s}^{\text{out}} = \frac{1}{2}\mathbf{A}\left[\begin{pmatrix}\chi^{XX} & \chi^{XY}\\ \chi^{YX} & \chi^{YY}\end{pmatrix}^* \otimes \begin{pmatrix}\chi^{XX} & \chi^{XY}\\ \chi^{YX} & \chi^{YY}\end{pmatrix}\right]\begin{bmatrix}1\\ \pm i\\ \mp i\\ 1\end{bmatrix} \quad (11)$$

Explicit evaluation yields the following expression

https://doi.org/10.1021/acs.jpcb.3c03104
J. Phys. Chem. B 2023, 127, 8216−8225

$$\mathbf{s}^{\text{out}} = \frac{1}{2}\begin{bmatrix} 1 & 0 & 0 & 1 \\ 1 & 0 & 0 & -1 \\ 0 & 1 & 1 & 0 \\ 0 & i & -i & 0 \end{bmatrix} \begin{bmatrix} (\chi^{XX^*}\chi^{XX} + \chi^{XY^*}\chi^{XY}) \pm \mathrm{i}(\chi^{XX^*}\chi^{XY} - \chi^{XY^*}\chi^{XX}) \\ (\chi^{XX^*}\chi^{YX} + \chi^{XY^*}\chi^{YY}) \pm \mathrm{i}(\chi^{XX^*}\chi^{YY} - \chi^{XY^*}\chi^{YX}) \\ (\chi^{YX^*}\chi^{XX} + \chi^{YY^*}\chi^{XY}) \pm \mathrm{i}(\chi^{YX^*}\chi^{XY} - \chi^{YY^*}\chi^{XX}) \\ (\chi^{YX^*}\chi^{YX} + \chi^{YY^*}\chi^{YY}) \pm \mathrm{i}(\chi^{YX^*}\chi^{YY} - \chi^{YY^*}\chi^{YX}) \end{bmatrix} \tag{12}$$

In eq 12, positive and negative signs indicate right and left circular polarizations, respectively. Simplification using the equalities between elements summarized in Table SII for macroscopically uniaxial assemblies yields the following expression for the Stokes vector.

$$\mathbf{s}^{\text{out}} = \begin{bmatrix} (\chi^{XX^*}\chi^{XX} + \chi^{YX^*}\chi^{YX}) \mp 2\mathrm{i}\chi^{YX^*}\chi^{XX} \\ 0 \\ 0 \\ \pm(\chi^{XX^*}\chi^{YY} - \chi^{YX^*}\chi^{YX}) - 2\mathrm{i}\chi^{YX^*}\chi^{XX} \end{bmatrix} \tag{13}$$

The CD response is connected to this expression through the following relation

$$\mathrm{CD} = A_{\mathrm{R}} - A_{\mathrm{L}} = -\log\left[\frac{s_0^{\text{out}}(\mathrm{R})}{s_0^{\text{out}}(\mathrm{L})}\right] = -\log\left[\frac{(\chi^{XX^*}\chi^{XX} + \chi^{YX^*}\chi^{YX}) - 2\mathrm{i}\chi^{YX^*}\chi^{XX}}{(\chi^{XX^*}\chi^{XX} + \chi^{YX^*}\chi^{YX}) + 2\mathrm{i}\chi^{YX^*}\chi^{XX}}\right] \tag{14}$$

Using the approximation $-\log(1 + x) \cong -x$ for $x \ll 1$ and assuming that the chiral-specific response is relatively small, the CD in eq 14 can be rewritten as the following

$$\mathrm{CD} \cong \frac{-2i\chi^{YX^*}\chi^{XX}}{|\chi^{XX}|^2 + |\chi^{YX}|^2} = \frac{2\mathrm{Im}(\chi^{YX^*}\chi^{XX})}{|\chi^{XX}|^2 + |\chi^{YX}|^2} \tag{15}$$

If one assumes a symmetric polarizability matrix consistent with a parametric process, the interchangeability of indices at the molecular level in $\boldsymbol{\alpha}$ translates to an analogous interchangeability of indices within each $\boldsymbol{\chi}$. This interchangeability simplifies the chiral-specific terms allowed within the electric dipole approximation for light to a single unique nonzero term; $f_{14}^* = f_{15}^* = f_{41} = f_{51}$ ($\chi^{XX}\chi^{XY*} = \chi^{XX}\chi^{YX*} = \chi^{XY*}\chi^{XX} = \chi^{YX*}\chi^{XX}$). With the additional symmetry constraint $f_{51} = -(f_{14} + f_{41} + f_{15}) = -(f_{15} + f_{51} + f_{15})$, simplification yields $f_{51} = -f_{15}$. The two combined relations $f_{15}^* = f_{51}$ and $f_{15} = -f_{51}$ suggest that only the imaginary contribution to $f_{51} = \chi^{YX*}\chi^{XX}$ describing optical transmission satisfies both equalities following orientational averaging and can, therefore, contribute to the chiral-specific CD response within the electric dipole approximation for light. Since the product $\chi^{YX*}\chi^{XX}$ must be purely imaginary by symmetry within the electric dipole approximation, the Im indication in eq 15 is formally superfluous but is included to aid in clarity in indicating a purely real-valued CD response.

Simplification of Electric-Dipole-Allowed CD for Planar Chromophores. The implications of eq 15 are worth explicitly evaluating in the limit of planar chromophores. Conjugation within organic chromophores strongly favors planar structures, such that the overwhelming majority of organic chromophores correspond to locally planar-conjugated structures. Furthermore, planar structures represent a minimal model; planar-conjugated ring systems explicitly contain a mirror-plane symmetry and are therefore nominally achiral but can nevertheless contribute to electric-dipole-allowed chiroptical effects in oriented assemblies. Applying the principle of Occam's razer, the assumption of planarity within the chromophore minimizes the required parameter space. Building on expressions derived previously for four-wave mixing spectroscopy for different molecular symmetries,[15] symmetry within the different molecular building blocks can greatly reduce the number of unique nonzero elements within the local tensor products. In the case of absorbance, the transition moment is defined by a vector, effectively reducing the resonance-enhanced contribution to the polarizability to a single internal dimension. For electronic spectroscopy of conjugated ring systems, it is often reasonable to assume that the low-energy electronic molecular polarizability is dominated by interactions within the plane of the chromophore, reducing the nonresonant polarizability to approximately two dimensions. If a coordinate system is selected for the molecular frame based on the principal moments of the nonresonant polarizability, only the two diagonal elements will be nonzero for a symmetric nonresonant polarizability matrix. This selection of local frame coordinates based on the nonresonant polarizability has the distinct advantage of varying slowly with wavelength, such that resonant features can be interpreted relative to this quasi-static internal reference frame. If the plane of the chromophore is defined as the (x',z') plane with the y'-axis orthogonal to the chromophore plane, only $\alpha_{\mathrm{NR}}^{x'x'}$ and $\alpha_{\mathrm{NR}}^{z'z'}$ remain within the nonresonant tensor.

$$\boldsymbol{\alpha}_{\mathrm{NR}} \in \{\alpha_{\mathrm{NR}}^{x'x'}, \alpha_{\mathrm{NR}}^{z'z'}\} \tag{16}$$

Assuming the transition moment lies within the same chromophore plane, the two principal nonresonant tensor elements in eq 16 are complemented by three unique resonant polarizability matrix elements, defined by the angle δ between the fixed principal nonresonant z'-axis and the wavelength-dependent resonant transition moment.

$$\boldsymbol{\alpha}_{\mathrm{R}} \in \begin{Bmatrix} \alpha_{\mathrm{R}}^{x'x'} = S_n(\omega)|\boldsymbol{\mu}_{n0}|^2 \sin^2\delta \\ \alpha_{\mathrm{R}}^{x'z'} = \alpha_{\mathrm{R}}^{x'z'} = S_n(\omega)|\boldsymbol{\mu}_{n0}|^2 \sin\delta\cos\delta \\ \alpha_{\mathrm{R}}^{z'z'} = S_n(\omega)|\boldsymbol{\mu}_{n0}|^2 \cos^2\delta \end{Bmatrix} \tag{17}$$

In eq 17, $S_n(\omega)$ describes the complex-valued lineshape function associated with resonance enhancement with state n. For Lorentzian lineshapes, $S_n(\omega) = (\hbar\omega_n - \hbar\omega - \mathrm{i}\hbar\Gamma_n)^{-1}$ from the first term eq 9, in which ω_n is the resonant frequency of the transition from the ground state to state n, ω is the incident frequency, and Γ_n is a damping constant describing the dissipative spectral peak shape. The squared magnitude of the transition moment in eq 17 arises from eq 9, bearing in mind that $\boldsymbol{\mu}_{0n}^* = \boldsymbol{\mu}_{n0}$. The total polarizability within the molecular frame is given locally by the coherent summation of

https://doi.org/10.1021/acs.jpcb.3c03104
J. Phys. Chem. B 2023, 127, 8216−8225

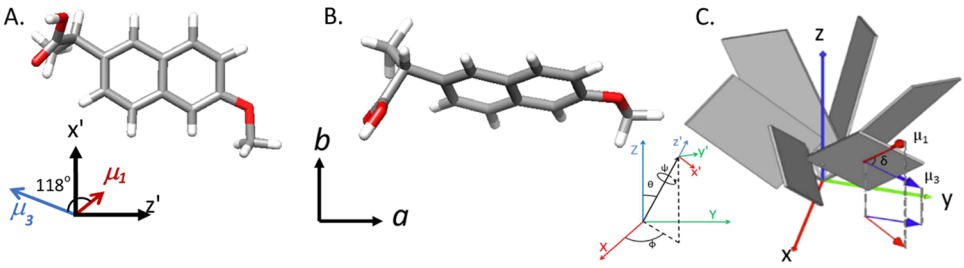

Figure 1. Structure of (*S*)-naproxen in the local (molecular) coordinate frame (A) and in the reference frame of the crystal (B), with the twofold screw axis oriented along the *b* crystallographic coordinate. Transformation between the two frames corresponds to a tilt angle of $\theta = 81°$ and twist $\psi = 155°$. Dynamic dipole transition moment orientations are shown for the two transitions dominating the predicted CD response, corresponding to the first (red) and third (blue) excited state transitions. Nonzero polar order in θ coupled with asymmetry in the distribution in twist angles ψ combine to enable electric-dipole-allowed chiral-specific CD spectroscopy through a geometric orientational mechanism depicted in panel (C) for uniaxial assemblies.

the resonant and nonresonant contributions. For different assumed lineshape functions (e.g., Gaussian or Voigt), the complex components do not adopt similarly concise forms but exhibit similar trends, all of which are constrained by causality to adhere to Kramers−Kronig relations.[18]

Simplification for a Pair of Uncoupled Oscillators. The expression in eq 8 simplifies considerably if the molecular transitions are dominated by just two closely spaced resonances to states *n* and *m*, which is a limiting case also considered previously by Salij et al.[6] In this limit, resonance with one of the two transitions generally includes overlapping nonresonant contributions from the other, and vice versa. If the *z*′-axis is defined coparallel with the transition moment for state *m*, $\alpha^{x'x'}$ becomes negligible and the nonresonant component of $\alpha^{z'z'}$ results in the following form for CD for Lorentzian lineshapes for resonance enhancement with state *n* for nonresonant polarizability dominated by a single energetically adjacent electronic transition with a resonance frequency of ω_m.

$$\begin{aligned}\mathrm{CD}_n &\propto \chi^{YX^*}\chi^{XX} \\ &= \frac{N_b|\boldsymbol{\mu}_{n0}|^2|\boldsymbol{\mu}_{m0}|^2}{2\hbar\varepsilon_0} \times \frac{\Gamma_n}{(\omega_n-\omega)^2+\Gamma_n^2} \\ &\quad \times \frac{(\omega_m-\omega)}{(\omega_m-\omega)^2+\Gamma_m^2} \times [\langle \sin^3\theta \sin\psi\rangle \sin\delta\cos\delta \\ &\quad + \langle \sin^2\theta\cos\theta\sin\psi\cos\psi\rangle \sin^2\delta] \end{aligned} \tag{18}$$

As one might expect, the roles of the two transitions invert upon consideration of resonance enhancement to state *m*.

$$\begin{aligned}\mathrm{CD}_m &\propto \chi^{YX^*}\chi^{XX} \\ &= \frac{N_b|\boldsymbol{\mu}_{n0}|^2|\boldsymbol{\mu}_{m0}|^2}{2\hbar\varepsilon_0} \times \frac{\Gamma_m}{(\omega_m-\omega)^2+\Gamma_m^2} \\ &\quad \times \frac{(\omega_n-\omega)}{(\omega_n-\omega)^2+\Gamma_n^2} \times [\langle \sin^3\theta \sin\psi\rangle \sin\delta\cos\delta \\ &\quad + \langle \sin^2\theta\cos\theta\sin\psi\cos\psi\rangle \sin^2\delta] \end{aligned} \tag{19}$$

Importantly, the sign must invert for the two CD responses due to the frequency difference in the numerator $[(\omega_n - \omega)$ versus $(\omega_m - \omega)]$. If the transition to state *m* lies higher in energy than to state *n*, CD_n will have a positive difference in the numerator when resonant with state *n* and a negative difference when resonant with state *m* and vice versa. Consequently, a pair of isolated transitions will produce a doublet in the CD spectrum. Unlike isotropic CD spectroscopy arising from magnetic dipoles produced from coupled oscillators, the electric dipole responses described above do not require energetic coupling between the two oscillators; the two transitions can appear in relatively remote and uncoupled regions within the molecular/macromolecular frame, as long as the plane defined by the two vectors exhibits net asymmetry in the distribution of the chromophore twist angle upon orientational averaging. Rotation of the substrate 180° about either the *X*- or *Y*-axes to invert the sample orientation relative to the optical axis inverts both of the two orientational averages given in eq 19 through 180° rotation in both θ and ψ. These predictions of the general framework are in excellent agreement with the predictions of Salij et al. in the limiting case of just two transitions contributing to the chiral-specific response.

RESULTS AND DISCUSSION

Prior to considering orientation effects at interfaces, baseline ultraviolet−visible (UV−vis) absorbance spectroscopy was performed for isotropic solutions of (*S*)-naproxen and compared with ab initio calculations. Relative internal orientations for the dominant low-lying transitions are indicated together with the molecular structure in Figure 1A. Isotropic averaging yields predicted isotropic spectra shown in Figure 2, together with experimental measurements for comparison. In brief, the quantum chemical calculations perform quite well in recovering the predicted linear absorption spectrum of solvated naproxen solutions. Specifically, both the excitation energies and the relative oscillator strengths of the major electronic absorption band around

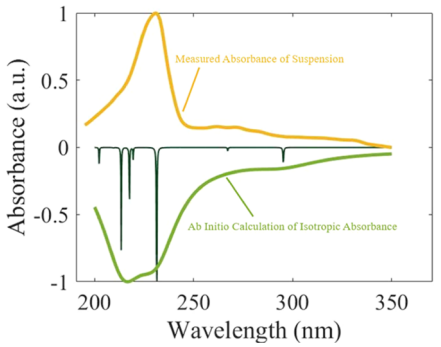

Figure 2. Comparison between the predicted isotropic absorbance spectrum of naproxen and the experimentally measured spectrum.

https://doi.org/10.1021/acs.jpcb.3c03104
J. Phys. Chem. B 2023, 127, 8216−8225

~230 nm and minor features around ~280 nm are in qualitatively good agreement with the experimental observations. The vibrational fine structure observed in the red-shifted transition is not reproduced in the electronic spectroscopy calculations, as the TD-DFT calculations operate within the constraints of the Born−Oppenheimer approximation. However, the major features and relative energies were nevertheless consistent with experimental trends.

Significant incoherent contributions to absorbance spectroscopy measurements require samples exhibiting local order extending over distances exceeding the optical wavelength. To assess the persistence length of orientational order, homochiral microcrystals of (*S*)-naproxen were prepared by drop-coating from a suspension in toluene. Brightfield images of the microcrystal presentation are shown in Figure 3. A spatial

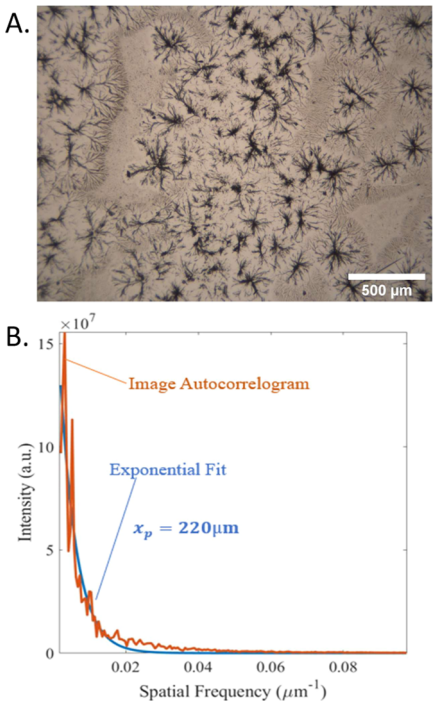

Figure 3. Optical micrograph (A) and spatial autocorrelogram (B) of drop-coated microcrystalline naproxen thin films, yielding a persistence length of order of x_p = 220 μm. Similar results were observed for persistence lengths evaluated just in the vertical and horizontal directions.

power spectrum of the brightfield image suggests characteristic feature sizes from a few μm out to ~400 μm. This length scale is substantially larger than the wavelength of light, suggesting a unique polarization and phase retardance from each individual microcrystal to produce a summation of transmitted intensities with substantial depolarization/incoherence. However, the characteristic feature size is nevertheless much smaller than the probe area of the spectrometer (~1 cm^2), suggesting integration over a statistically uniform population of particle azimuthal orientations. These combined conditions are in excellent agreement with the macroscopic sample requirements of the theoretical framework for incoherent summation over a net uniaxial macroscopic distribution.

Notably, the ab initio calculations with no adjustable parameters correctly recover both the relative signs and amplitudes of the major spectral features in the CD measurements of naproxen microcrystalline thin films, as well as the sign inversion upon substrate reorientation. Figure 4 contains ab initio calculations and experimental measurements

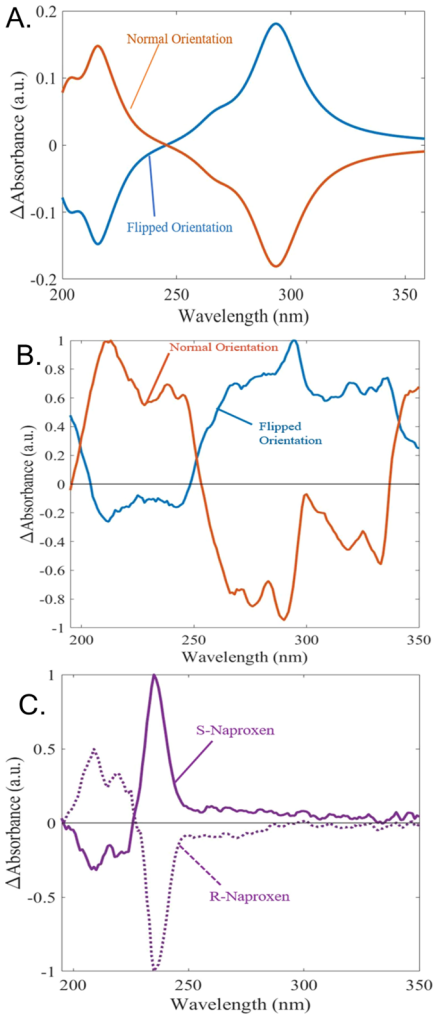

Figure 4. Predicted CD spectrum of a (*S*)-naproxen thin film upon sample flipping (A), the experimentally measured spectra of (*S*)-naproxen in normal and flipped orientations (B), and the CD spectrum of the crystalline suspension (C).

of the CD response expected for homochiral naproxen microcrystals. Calculations shown in Figure 4A were based on the known molecular structure of (*S*)-naproxen based on the X-ray structure and the naproxen orientation within the crystalline lattice. The $P2_1$ twofold screw axis symmetry of the lattice effectively results in rotational optical symmetry about the crystallographic *b*-axis. Predictions are shown for a crystallographic *b*-axis preferentially oriented either coparallel or antiparallel with the spectrometer optical axis. The results of the calculations are in excellent agreement with experimental measurements for interfacial assemblies of (*S*)-naproxen microcrystals oriented at a hydrophilic fused silica interface, as shown in Figure 4B. Assemblies prepared with (*R*)-naproxen produced films exhibiting similar trends but inverted in sign. Similar CD spectra in sign and peak locations were obtained from multiple fields of view within a given sample and across multiple independently prepared samples with different persistence lengths of order x_p. The long-wavelength portion of the spectrum is dominated by a doublet, consisting of a broad band with a vibronic progression extending from 260 to

https://doi.org/10.1021/acs.jpcb.3c03104
J. Phys. Chem. B 2023, 127, 8216−8225

340 nm and a nominally sign-inverted feature centered at 230 nm. The electronic absorption spectrum of naproxen is well established to exhibit clear vibronic progressions,[23] resulting in periodic series of peaks for each electronic transition. The presence of two low-lying and spectrally overlapping electronic transitions in the absorption spectrum of naproxen is consistent with prior calculations[24] and experiments[25] for naphthalene and related derivatives. Notably, these red-shifted spectral features from 260 to 340 nm contribute negligibly to the CD response acquired in both solutions and microcrystalline suspensions, as shown in Figure 4C. A strong feature at 235 nm dominating the isotropic CD response is both predicted and observed to generate CD response approximately equal in magnitude and opposite in sign to the red-shifted peak in the oriented microcrystalline thin films. As the quantum chemical calculations were all performed within the Born−Oppenheimer approximation, they did not capture the vibronic progression of peaks red-shifted from the electronic origins. However, the signs, magnitudes, and energies of the assigned pure electronic transitions agreed remarkably well with experimental observations.

Inspection of the electronic structure calculations further supports the proposed chiral-specific origin of the observed CD spectroscopy for oriented naproxen microcrystals. The lowest lying electronic transition calculated to be centered around ∼290 nm is dominated by the highest occupied molecular orbital (HOMO) → lowest unoccupied molecular orbital (LUMO). For this transition, both molecular orbitals are highly localized to the nominally planar naphthalene ring with negligible orbital density on the chiral carbon or carboxylic acid group (see the Supporting Information). These calculations are consistent with minimal CD activity observed in isotropic solutions and microcrystalline suspensions for this low-lying electronic state. In contrast, the higher energy feature centered at ∼225 nm in the ab initio calculations is dominated by the HOMO → LUMO + 3 orbitals, which is dominated by a charge-transfer transition shifting electron density from the ring system across the chiral center to the carboxylic acid group.

Despite the absence of isotropic chirality within the nominally planar HOMO−LUMO transition, the proposed orientational mechanism does not require intrinsic chirality within the chromophore itself to generate large dissymmetry parameters in absorbance CD. In the limit of a two-state system described in eqs 18 and 19, electric-dipole-allowed CD can arise from a pair of transitions defining the chromophore plane if they satisfy three conditions: (i) the two transition moments are not coparallel, and (ii) the molecular orientation distribution exhibits net polar order, and (iii) the plane defined by the two transition moments exhibits asymmetry in the twist angle ψ. The transition moments for the two electronic transitions dominating the accessible UV−vis spectrum are depicted by the red and blue vectors in Figure 1A and produce a calculated internal angle from eq 18 of $\delta = 118°$, satisfying the first requirement. Assuming a crystal orientation with the polar twofold screw axis coparallel or antiparallel to the surface, the second requirement is also satisfied. In this crystal orientation, the twist angle connecting the molecular frame to the laboratory frame is $\psi = 155°$, satisfying the third requirement. Consequently, no chirality is required in the internal plane defined by the two vectors μ_1 and μ_3 for the prediction of nonzero CD, provided chiral-specific interactions driving the molecular orientation within the lattice produce net polar order and a net asymmetry in the twist angle of that same internal plane relative to the interface normal.

Comparison of CD spectroscopy of intact microcrystals in suspension and for the drop-coated samples highlights the significance of orientational order in the macroscopic spectral observables. Optical transmission measurements performed on naproxen microcrystals suspended in hexanes are expected to produce comparable optical decoherence on a per-particle basis as those same microcrystals following deposition onto a hydrophilic substrate. Nevertheless, the orientational averaging for an isotropic suspension is predicted to produce zero-valued CD activity within the electric dipole approximation according to eqs 18 and 19. In this limit, only the much weaker isotropic chirality remains. Consistent with this prediction, the CD activity of the isotropic suspension is nearly identical to that observed for naproxen solutions (S2), dominated by the blue-shifted features closely associated with electronic resonances around 235 nm spanning the chiral center.

The ab initio calculations were performed assuming a specific crystallographic orientational preference at the interface, which has the potential to bias the calculations if different orientation distributions are adopted experimentally. Drop-coating is generally expected to favor crystal orientations with more hydrophilic exposed crystal faces oriented toward the substrate interface. The role of crystal orientation was explored by repeating the simulations for several different assumed crystal orientations. Qualitatively, similar results were obtained for crystal orientations for b-axis tilt angles of $0° \leq \theta < \sim 45°$ (irrespective of the crystal twist angle ψ). Crystal orientations with $\theta \cong 90°$ resulted in the loss of all electric-dipole-allowed CD activity. This result is entirely expected given the twofold screw axis symmetry of the crystal; orientation of the crystal axis at 90° produces films unchanged by sample reorientation upon flipping of the substrate. As such, the measured CD response is likely dominated by the subset of crystals exhibiting preferential polar orientation of the crystallographic b-axis.

The absolute sign of the measured CD response for a given orientation of the substrate in the instrument should depend on crystal orientation at the interface. Given the prominent role of the primitive (010) and $(0\bar{1}0)$ planes in CD spectroscopy of naproxen crystals by nature of the $P2_1$ crystal symmetry, it is worthwhile considering the relative interfacial free energies of the two opposing crystal faces and the possible driving forces responsible for possible preferred crystallographic orientation. Notably, the carboxylic acid functional group preferentially orients antiparallel with the crystallographic b-axis depicted in Figure 1B, corresponding to the twofold screw axis. Screw dislocation about the b-axis preserves an antiparallel orientation of the carboxylic acid group. Assuming the carboxylic acid-terminated $(0\bar{1}0)$ plane is likely to be significantly more hydrophilic than the opposing methyl-terminated (010) primitive lattice planes, it is correspondingly reasonable to expect crystallographic orientations with the $(0\bar{1}0)$ plane preferentially oriented toward the glass substrate, and the (010) plane oriented toward toluene/air. The result of this assumed orientation shown in Figure 1 correctly recovers the absolute sign of the experimentally measured CD response from the ab initio calculations, again with no adjustable parameters. Despite the admitted oversimplifications used in the quantum chemical calculations, the general agreement between the predicted and measured CD spectra was quite striking, given that all calculations were performed exclusively within the electric dipole approximation for light. As such, it is

https://doi.org/10.1021/acs.jpcb.3c03104
J. Phys. Chem. B 2023, 127, 8216−8225

reasonable to conclude that the proposed minimal model nevertheless effectively captures the key major driving interactions underpinning the molecular/macromolecular origins of nonreciprocal CD.

The theoretical framework presented herein derived from the extension of coherent four-wave mixing formalism to incoherent two-wave mixing is in good qualitative agreement with the predictions of the prior model by Salij et al.[6] Both models require an interplay between complex-valued components in the polarizability, as illustrated by consideration of internal planes defined by transition moment pairs in two-state systems. In this two-state limit, electric-dipole-allowed nonreciprocal CD can arise from planar chromophores exhibiting a right-handed or left-handed rotation between the blue- and red-shifted transitions projected onto the surface plane. The model herein specifically considers the molecular orientation distribution driving that projected shift based on a formal assumption of macroscopic C_∞-symmetry, connecting the CD back to supramolecular chiral arrangement of nominally achiral chromophores. However, the general features of the present and prior considerations are in remarkably good agreement.

The mathematical relations describing CD spectroscopy of ordered assemblies reveal important symmetry relations. First, observation of nonreciprocal CD within uniaxial assemblies requires sample chirality. Increasing symmetry from C_∞ to $C_{\infty v}$, D_∞, or $D_{\infty h}$ through the addition of mirror-plane symmetry operations results in the removal of the tensor products responsible for observation of nonreciprocal CD within the electric dipole approximation. Second, the theoretical CD dissymmetry parameters from the incoherent transmission can approach unity, as they are fully electric-dipole-allowed in uniaxial assemblies. Third, nonreciprocal CD from the incoherent component of the optical transmission is interface-specific, disappearing by symmetry in systems lacking polar order. Finally, chirality is not required within the nominally planar chromophores driving the CD response, provided the chromophore planes adopt supramolecular arrangements with both chiral asymmetry in the twist angle of the chromophore planes and net polar order. These collective symmetry-dependent results suggest potentially interesting applications of CD for chiral-specific and interface-specific spectroscopy of uniaxially ordered assemblies.

The attribution of this work to large chiral-specific effects from nominally planar chromophores through orientational ordering is in excellent agreement with prior observations of chiral-specific spectroscopic observables. Kahr and co-workers elegantly summarize chiroptical spectroscopy of planar molecular assemblies through anisotropic crystal orientation.[26] In second-harmonic and sum-frequency spectroscopies, orientational contributions of nominally planar chromophores to chiral-specific surface spectroscopy are well established both theoretically[27] and experimentally.[28−30] In a noteworthy example, chiral orientation was used to interpret vibrational chiroptical sum-frequency spectroscopy of planar water molecules oriented by biomolecular interactions.[30,31]

The applicability of this four-wave mixing mathematical framework for predicting and describing large chiroptical effects in absorption spectroscopy suggests a possible further extension to polarization-dependent microscopy measurements. Samples amenable to optical imaging as a rule contain features with persistence lengths greater than the optical wavelength to produce optical contrast. In such instances, observations of localized CD from uniaxial assemblies may potentially arise from LD−LB interactions that are interpretable within the context of the proposed orientational model. Indicators for local CD arising from LD−LB coupling would include (i) CD activities potentially much larger than observed for isotropic measurements of similar molecular building blocks and (ii) sign inversion for different domains with the same intrinsic chirality but differing polar order.

Interestingly, observations consistent with both indicators above have recently been reported in vibrational circular dichroism (VCD) imaging measurements by Phal, Yeh, and Bhargava.[32] In that work, Phal et al. reported ∼1000-fold enhancements in the dissymmetry parameters ($\Delta A = A_L - A_R \cong \pm 2\%$) in VCD microscopy measurements of dehydrated colon tissue sections relative to analogous measurements made on disordered thin protein films. In addition, the absolute signs of the VCD ratios inverted within different domains (e.g., within healthy versus tumorous tissues). These sign disparities were tentatively attributed to differences in α-helical versus β-sheet content within the different tissue domains.[32] However, the 1000-fold increase in ΔA and sign inversion within different spatial regions suggest the potential for electric-dipole-allowed orientational contributions supplementing or superseding the relatively weak magnetic dipole contributions that dominate disordered assemblies. If the VCD observables from such samples are found to be driven by chiral-specific LD−LB effects, the mathematical framework presented herein can potentially aid in bridging those polarization-dependent microscopic measurements back to the molecular structure and orientation in the local frame of the sample. This specific example is representative of what we hope to be a general tool, in which the proposed conceptual framework provides a relatively simple molecular understanding of polarization-dependent spectroscopy and microscopy measurements of microscopically structured chiral assemblies.

■ ASSOCIATED CONTENT

Supporting Information

The Supporting Information is available free of charge at https://pubs.acs.org/doi/10.1021/acs.jpcb.3c03104.

Details on symmetry-allowed tensor products for uniaxial assemblies, geometry-related simplifications used for calculations of naproxen CD spectrum, algorithm connecting quantum chemical calculations to surface response, and additional absorbance and CD measurements (PDF)

■ AUTHOR INFORMATION

Corresponding Author

Garth J. Simpson − *Department of Chemistry, Purdue University, West Lafayette, Indiana 47907, United States;* orcid.org/0000-0002-3932-848X; Email: gsimpson@purdue.edu

Authors

Gwendylan A. Turner − *Department of Chemistry, Purdue University, West Lafayette, Indiana 47907, United States*

Yechan Hwang − *Department of Chemistry, Purdue University, West Lafayette, Indiana 47907, United States*

Jiayue Rong − *Department of Chemistry, Purdue University, West Lafayette, Indiana 47907, United States*

Camila Strachan − *Department of Chemistry, Purdue University, West Lafayette, Indiana 47907, United States*

Complete contact information is available at:
https://pubs.acs.org/10.1021/acs.jpcb.3c03104

Notes

The authors declare no competing financial interest.

■ ACKNOWLEDGMENTS

The authors gratefully acknowledge funding from the National Science Foundation (NSF-D3SC-2004046). G.AT. also acknowledges support from the NSF Center for Bioanalytic Metrology (IIP-1916691). This work was supported in part by the Research Instrumentation Center in the Department of Chemistry at Purdue University.

■ REFERENCES

(1) Freudenthal, J. H.; Hollis, E.; Kahr, B. Imaging Chiroptical Artifacts. *Chirality* **2009**, *21*, E20−E27.
(2) Maestre, M. F.; Katz, J. E. A Circular Dichroism Microspectrophotometer. *Biopolymers* **1982**, *21*, 1899−1908.
(3) Shindo, Y.; Nishio, M.; Maeda, S. Problems of CD Spectrometers (V): Can We Measure CD and LD Simultaneously? Comments on Differential Polarization Microscopy (CD and Linear Dichroism). *Biopolymers* **1990**, *30*, 405−413.
(4) Albano, G.; Pescitelli, G.; di Bari, L. Chiroptical Properties in Thin Films of π-Conjugated Systems. *Chem. Rev.* **2020**, *120*, 10145−10243.
(5) Shindo, Y. Application of Polarized Modulation Technique in Polymer Science. *Opt. Eng.* **1995**, *34*, 3369−3384.
(6) Salij, A.; Goldsmith, R. H.; Tempelaar, R. Theory of Apparent Circular Dichroism Reveals the Origin of Inverted and Noninverted Chiroptical Response under Sample Flipping. *J. Am. Chem. Soc.* **2021**, *143*, 21519−21531.
(7) Albano, G.; Lissia, M.; Pescitelli, G.; Aronica, L. A.; di Bari, L. Chiroptical Response Inversion upon Sample Flipping in Thin Films of a Chiral Benzo[1,2-b:4,5-B′]Dithiophene-Based Oligothiophene. *Mater. Chem. Front.* **2017**, *1*, 2047−2056.
(8) von Weber, A.; Hooper, D. C.; Jakob, M.; Valev, V. K.; Kartouzian, A.; Heiz, U. Circular Dichroism and Isotropy − Polarity Reversal of Ellipticity in Molecular Films of 1,1′-Bi-2-Naphtol. *ChemPhysChem* **2019**, *20*, 62−69.
(9) Ristow, F.; Liang, K.; Pittrich, J.; Scheffel, J.; Fehn, N.; Kienberger, R.; Heiz, U.; Kartouzian, A.; Iglev, H. Large-Area SHG-CD Probe Intrinsic Chirality in Polycrystalline Films. *J. Mater. Chem. C* **2022**, *10*, 12715−12723.
(10) Azzam, R. M. A.; Bashara, N. M. *Ellipsometry and Polarized Light*; Elsevier: Amsterdam, 1987.
(11) Saleh, B. E. A.; Teich, M. C. *Fundamentals of Photonics*; John Wiley & Sons: New York, 1991.
(12) Clays, K.; Persoons, A. Hyper-Rayleigh Scattering in Solution. *Phys. Rev. Lett.* **1991**, *66*, 2980.
(13) Bersohn, R.; Pao, Y. H.; Frisch, H. L. Double-Quantum Light Scattering by Molecules. *J. Chem. Phys.* **1966**, *45*, 3184.
(14) Simpson, G. J. *Nonlinear Optical Polarization Analysis in Chemistry and Biology*; Camgridge Molecular Science, 2017.
(15) Davis, R. P.; Moad, A. J.; Goeken, G. S.; Wampler, R. D.; Simpson, G. J. Selection Rules and Symmetry Relations for Four-Wave Mixing Measurements of Uniaxial Assemblies. *J. Phys. Chem. B* **2008**, *112*, 5834−5848.
(16) Long, D. A. *The Raman Effect. A Unified Treatment of the Theory of Raman Scattering by Molecules*; John Wiley & Sons: New York, 2002.
(17) Deng, F.; Ulcickas, J. R. W.; Simpson, G. J. Theoretical Foundation for Electric-Dipole-Allowed Chiral-Specific Fluorescence Optical Rotary Dispersion (F-ORD) from Interfacial Assemblies. *J. Phys. Chem. Lett.* **2016**, *7*, 4248−4252.
(18) Kronig, R. d. L. On the Theory of Dispersion of X-rays. *J. Opt. Soc. Am.* **1926**, *12*, 547−557.
(19) Barca, G. M. J.; Bertoni, C.; Carrington, L.; Datta, D.; de Silva, N.; Deustua, J. E.; Fedorov, D. G.; Gour, J. R.; Gunina, A. O.; Guidez, E.; et al. M. S. Recent Developments in the General Atomic and Molecular Electronic Structure System. *J. Chem. Phys.* **2020**, *152*, No. 154102.
(20) Groom, C. R.; Bruno, I. J.; Lightfoot, M. P.; Ward, S. C. The Cambridge Structural Database. *Acta Crystallogr., Sect. B: Struct. Sci., Cryst. Eng. Mater.* **2016**, *72*, 171−179.
(21) Ravikumar, B. K.; Rajan, S. S.; Pattabhi, V.; Gabe, E. J. Structure of Naproxen, C14H14O3. *Acta Crystallogr., Sect. C: Cryst. Struct. Commun.* **1985**, *41*, 280−282.
(22) Bode, B. M.; Gordon, M. S. Macmolplt: A Graphical User Interface for GAMESS. *J. Mol. Graphics Modell.* **1998**, *16*, 133−138.
(23) Luber, S.; Neugebauer, J.; Reiher, M. Enhancement and De-Enhancement Effects in Vibrational Resonance Raman Optical Activity. *J. Chem. Phys.* **2010**, *132*, No. 044113.
(24) Adachi, M.; Murata, Y.; Nakamura, S. Spectral Similarity and Difference of Naphthalenetetracarboxylic Dianhydride, Perylenetetracarboxylic Dianhydride, and Their Derivatives. *J. Phys. Chem. A* **1995**, *99*, 14240−14246.
(25) Yamaguchi, H.; Kitano, K.; Toyoda, K.; Baumann, H. Magnetic Circular Dichroism Spectra of Naphthalic Anhydride and 1,4,5,8-Naphthalenetetracarboxylic 1,8:4,5-Dianhydride. *Spectrochim. Acta, Part A* **1982**, *38*, 261−263.
(26) Martin, A. T.; Nichols, S. M.; Murphy, V. L.; Kahr, B. Chiroptical Anisotropy of Crystals and Molecules. *Chem. Commun.* **2021**, *57*, 8107−8120.
(27) Simpson, G. J. Structural Origins of Circular Dichroism in Surface Second Harmonic Generation. *J. Chem. Phys.* **2002**, *117*, 3398−3410.
(28) Wampler, R. D.; Simpson, J. G.; et al. Mechanism of the Chiral SHG Activity of Bacteriorhodopsin Films. *J. Am. Chem. Soc.* **2006**, *128*, 10994−10995.
(29) Wang, J.; Chen, X.; Clarke, M. L.; Chen, Z. Detection of Chiral Sum Frequency Generation Vibrational Spectra of Proteins and Peptides at Interfaces in Situ. *Proc. Natl. Acad. Sci. U.S.A.* **2005**, *102*, 4978−4983.
(30) McDermott, M. L.; Vanselous, H.; Corcelli, S. A.; Petersen, P. B. DNA's Chiral Spine of Hydration. *ACS Cent. Sci.* **2017**, *3*, 708−714.
(31) Nagata, Y.; Bonn, M. Biomolecular Chirality Is Imprinted on One Layer of Hydration Water. *ACS Cent. Sci.* **2022**, *8*, 1380−1382.
(32) Phal, Y.; Yeh, K.; Bhargava, R. Concurrent Vibrational Circular Dichroism Measurements with Infrared Spectroscopic Imaging. *Anal. Chem.* **2021**, *93*, 1294−1303.